EPJ Web of Conferences **90**, 06002 (2015)
DOI: 10.1051/epjconf/ 20159006002

Minireview on diffraction

Gösta Gustafson[1,a]

[1] *Dept. of Astronomy and Theoretical Physics, Lund University*
Sölvegatan 14A, 22362 Lund, Sweden

Abstract. A short review is presented on diffractive excitation in high energy collisions.

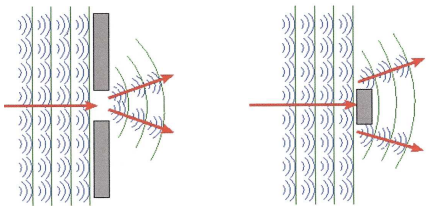

Figure 1. In optics a hole is equivalent to a black absorber.

1 Content

1. Optical analogy and Good–Walker formalism
2. Soft diffraction
   - Reggeon theory
   - QCD and the BFKL pomeron
3. Hard diffraction

2 Optical analogy and Good–Walker

In diffraction in optics, a hole is equivalent to a black absorber, with a forward peak with an angular width $\theta \sim \lambda/$(opening width), see fig. 1. Rescattering is described by a convolution in transverse momentum space, which corresponds to a product in transverse coordinate space. This implies that diffraction and rescattering is more easily described in impact parameter space.

The optical theorem says that

$$\mathrm{Im}\, A_{el} = \frac{1}{2}\{|A_{el}|^2 + \sum_j |A_j|^2\}. \qquad (1)$$

Here the sum runs over all inelastic channels j. For a structureless projectile (*e.g.* a photon), diffraction corresponds to elastic scattering driven by absorption. If the absorption probability in Born approximation is given by $2F$, then rescattering exponentiates in **b**-space, giving

$$d\sigma_{inel}/d^2b = 1 - e^{-2F}, \qquad (2)$$

and the optical theorem in eq. (1) gives:

$$\mathrm{Im}\, A_{el} = 1 - e^{-F} \qquad (3)$$

$$d\sigma_{el}/d^2b = (1 - e^{-F})^2 \qquad (4)$$

$$d\sigma_{tot}/d^2b = 2(1 - e^{-F}). \qquad (5)$$

Diffractive excitation

As an example we can look at a photon in an optically active medium. Here righthanded and lefthanded photons move with different velocities, meaning that they propagate as particles with different mass. Study a beam of righthanded photons hitting a polarized target, which absorbes photons polarized in the x-direction. The diffractively scattered beam is then a mixture of right- and lefthanded photons. If the righthanded photons have lower mass, this means that *the diffractive beam contains also photons excited to a state with higher mass*.

Good–Walker formalism

For a projectile with a substracture, the mass eigenstates can differ from the eigenstates of diffraction. Call the diffractive eigenstates Φ_n, with elastic scattering amplitudes T_n. The mass eigenstates Ψ_k are linear combinations of the states Φ_n:

$$\Psi_k = \sum_n c_{kn}\Phi_n \quad (\text{with } \Psi_{in} = \Psi_1). \qquad (6)$$

The elastic scattering amplitude is given by

$$\langle\Psi_1|T|\Psi_1\rangle = \sum c_{1n}^2 T_n = \langle T\rangle, \qquad (7)$$

and the elastic cross section

$$d\sigma_{el}/d^2b = (\sum c_{1n}^2 T_n)^2 = \langle T\rangle^2. \qquad (8)$$

The amplitude for diffractive transition to the mass eigenstate Ψ_k is given by

$$\langle\Psi_k|T|\Psi_1\rangle = \sum_n c_{kn} T_n c_{1n}, \qquad (9)$$

[a] e-mail: gosta.gustafson@thep.lu.se

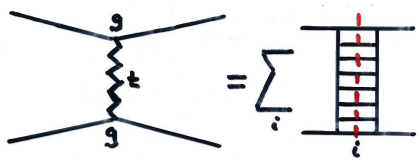

Figure 2. Ladder diagram related to pomeron exchange.

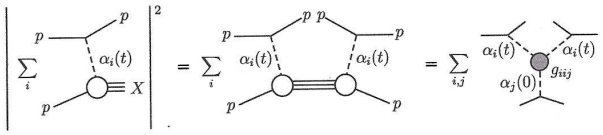

Figure 3. Mueller triple-Regge diagram. (Figure from ref. [1].)

which gives a total diffractive cross section (including elastic scattering)

$$d\sigma_{diff}/d^2b = \sum_k \langle\Psi_1|T|\Psi_k\rangle\langle\Psi_k|T|\Psi_1\rangle = \langle T^2\rangle. \quad (10)$$

Consequently the cross section for diffractive excitation is *given by the fluctuations*:

$$d\sigma_{diff\,ex}/d^2b = d\sigma_{diff} - d\sigma_{el} = \langle T^2\rangle - \langle T\rangle^2. \quad (11)$$

3 Soft diffraction

3.1 Reggeon theory

Pomeron exchange is described by a ladder exchanged between the projectile and the target, as illustrated in fig. 2. The elastic and total cross sections are given by

$$d\sigma_{el}/dt \sim (g^2 \cdot s^{\alpha(t)-1})^2 = g^4 s^{2(\alpha(0)-1)} e^{2(\ln s)\alpha' t} \quad (12)$$

$$\sigma_{tot} \sim g^2 s^{\alpha(0)-1} \quad (13)$$

Note that $\alpha(0) > 1$ implies that $\sigma_{el} > \sigma_{tot}$ for large s, which means that multi-pomeron exchange must be important.

Inelastic diffraction is described by the Mueller triple-Regge formalism, illustrated in fig. 3. The triple-pomeron contribution to the cross section is given by

$$\sigma \sim g_{pP}^2(t) g_{pP}(0) g_{3P} \left(\frac{s}{M_X^2}\right)^{2(\alpha(t)-1)} \left(M_X^2\right)^{(\alpha(0)-1)}, \quad (14)$$

where g_{3P} denotes the triple-pomeron coupling.

The triple (and multiple) pomeron couplings give loops, as illustrated in fig. 4, which leads to complicated resummation schemes. The diagrams can also contain multipomeron vertices, see fig. 5.

In particular three groups have studied these problems: Tel Aviv (GLM) [2], Durham (KMR) [3], and Ostapchenko [4] (based on work by Kaidalov and coworkers). In this approach low-mass diffraction is included with the Good–Walker formalism, approximated by one excited state N^*, while high-mass diffraction is treated with the triple-regge formalism. At lower energies or excitations

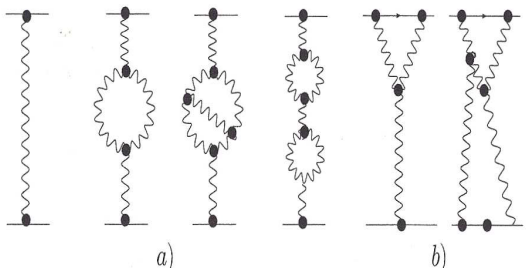

Figure 4. Examples of pomeron loop diagrams (copied from the Tel-Aviv group).

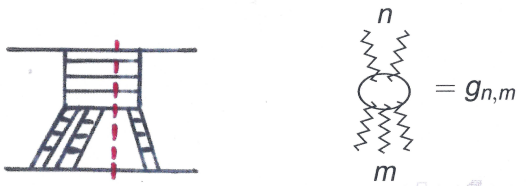

Figure 5. Multi-pomeron vertices. *Left*: A cut through an event with diffractive excitation. *Right*: A vertex with coupling between n and m pomerons.

also reggeons with $\alpha(0) \approx 0.5$ are included besides the pomeron. The regge intercepts and couplings are fitted to experimental data. We note here that these fits have been significantly modified after the presentation of the Totem data at 7 TeV, with $\sigma_{tot} = 98.6 \pm 2.2$ mb and $\sigma_{el} = 25.4 \pm 1.1$ mb [5].

- The *Tel-Aviv* group [2] has a single pomeron, with $\alpha_P(0) = 1.23$ and $\alpha' \approx 0$. This implies that the pomeron propagator is approximately a delta-function, $\delta(\mathbf{b})$, with no diffusion in $\mathbf{b}$-space. Only 3-pomeron vertices are included.
- The *Durham* group [3] has in its new version from 2014 a single "effective" pomeron with couplings dependent on $k_\perp$. It interpolates between a "bare $\boldsymbol{P}$" with $\alpha_P(0) \approx 1.3$ and α' small, and a "soft $\boldsymbol{P}$" with $\alpha_P(0) \approx 0.08$ and $\alpha' = 0.25$. Multi-pomeron couplings are large, with $g_{n,m} \propto n\,m\,\gamma^{n+m}$.
- *Ostapchenko* [4] has a formalism with two pomerons, with $\alpha_P(0)_{soft} = 1.14$ and $\alpha_P(0)_{hard} = 1.31$. The multi-pomeron couplings are fixed by the relation $g_{n,m} \propto \gamma^{n+m}$, and thus not growing with n and m as fast as assumed by the Durham group.

The results obtained for the single diffractive cross section are presented in fig. 6, reproduced from Cartiglia [6]. The different experiments have different acceptance range in M_X, and adjusting for this there is a general agreement between the results. We note in particular that Atlas and CMS have similar results, and also that these high energy results agree with tunes presented after the presentation of cross section data from Totem.

The models can also reproduce the dependence on the excitation mass M_X. As an example fig. 7 shows

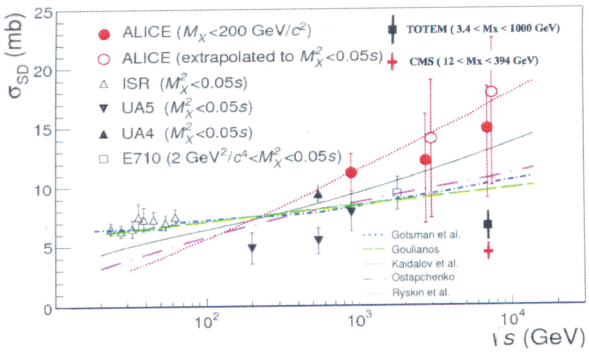

Figure 6. Single diffractive cross sections, compared with models. Figure from ref. [6].

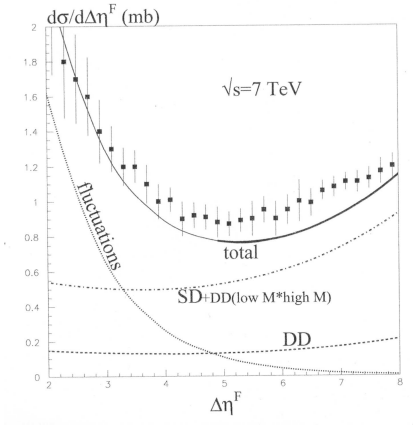

Figure 7. $d\sigma/d\eta^F \sim d\sigma/d\ln M_X^2$. Data from Atlas [7] and model calculations from ref. [3].

$d\sigma/d\eta^F \sim d\sigma/d\ln M_X^2$ from KMR compared with data from Atlas.

3.2 QCD and the BFKL pomeron

Mueller's dipole model

As mentioned above, unitarity constraints and saturation are much easier to account for in transverse coordinate space. Mueller's dipole model [8, 9] is a formulation of LL BFKL evolution in impact parameter space. A color charge is always screened by an accompanying anticharge. A charge-anticharge pair can emit bremsstrahlung gluons in the same way as an electric dipole. The probability per unit rapidity for a dipole $(\mathbf{r}_0, \mathbf{r}_1)$ to emit a gluon in the point $\mathbf{r}_2$, is given by (*cf* fig. 8)

$$\frac{d\mathcal{P}}{dy} = \frac{\bar{\alpha}}{2\pi} d^2\mathbf{r}_2 \frac{r_{01}^2}{r_{02}^2\, r_{12}^2}. \tag{15}$$

The important difference from electro-magnetism is that the emitted gluon carries away colour, which implies that the dipole splits in two dipoles. These dipoles can then emit further gluons in a cascade, producing a chain of dipoles as illustrated in fig. 8.

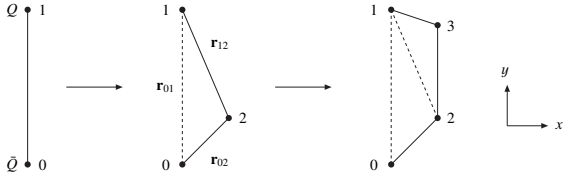

Figure 8. A colour dipole cascade in transverse coordinate space. A dipole can radiate a gluon. The gluon carries away colour, which implies that the dipole is split in two dipoles, which in the large N_c limit radiate further gluons independently.

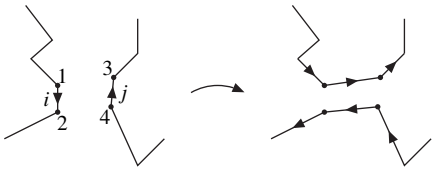

Figure 9. In a collision between two dipole cascades, two dipoles can interact via gluon exchange. As the exchanged gluon carries colour, the two dipole chains become recoupled.

When two such chains, accelerated in opposite directions, meet, they can interact via gluon exchange. This implies exchange of colour, and thus a reconnection of the chains as shown in fig. 9. The elastic scattering amplitude for gluon exchange is in the Born approximation given by

$$f_{ij} = \frac{\alpha_s^2}{2} \ln^2\left(\frac{r_{13}r_{24}}{r_{14}r_{23}}\right). \tag{16}$$

BFKL evolution is a stochastic process, and many subcollisions may occur independently. Summing over all possible pairs gives the total Born amplitude

$$F = \sum_{ij} f_{ij}. \tag{17}$$

The uniterized amplitude becoms

$$T = 1 - e^{-\sum f_{ij}}, \tag{18}$$

and the cross sections

$$d\sigma_{el}/d^2b = T^2, \qquad d\sigma_{tot}/d^2b = 2T \tag{19}$$

The Lund cascade model DIPSY

The DIPSY model [10–12] is a generalization of Mueller's cascade, which includes a set of corrections:

- Important non-leading effects in BFKL evolution. Most essential are those related to energy conservation and running α_s.
- Saturation from pomeron loops in the evolution. Dipoles with identical colours form colour quadrupoles, which give pomeron loops in the evolution. These are not included in Mueller's model or in the BK equation.
- Confinement via a gluon mass satisfies t-channel unitarity.

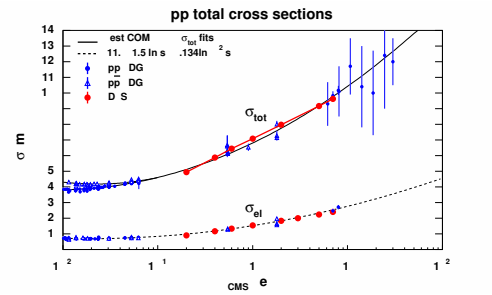

Figure 10. DIPSY results for total and elastic pp cross sections, compared to experimental data.

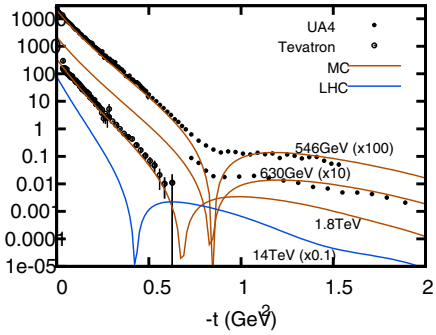

Figure 11. DIPSY results for the differential elastic pp cross section.

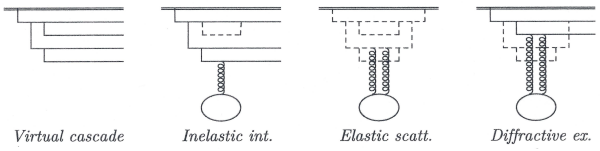

Figure 12. The virtual BFKL cascades are assumed to represent eigenstates for diffractive scattering. When they interact with a target, it can be absorbed in an inelastic event, give elastic scattering or diffractive excitation.

- The DIPSY MC gives also fluctuations and correlations.
- It can be applied to collisions between electrons, protons, and nuclei.

Some results for pp total and elastic cross sections are shown in figs. 10, 11 [13]. (Here the initial proton wave function is approximated by three dipoles in a triangle.) We note that there is no input structure functions in the model; the gluon distributions are generated within the model.

Good–Walker *vs* triple–regge

It is natural to assume that the diffractive eigenstates for a colliding proton are the BFKL cascades, which can come on shell through interaction with the target, as illustrated in fig. 12, *cf* refs. [14–17].

These diffractive states have a continuous distribution up to high masses, with large fluctuations. As demonstrated in ref. [18], calculating diffractive excitation via

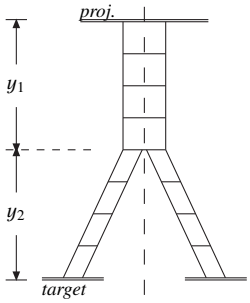

Figure 13. Triple-pomeron diagram, with $s = \exp(y_1 + y_2)$ and $M_X^2 = \exp(y_1)$.

the Good–Walker or the triple-regge formalism, is just different formulations of the same phenomenon. An essential feature of the BFKL cascade is its stochastic nature. If the probability for a dipole split is given by $dP/dy \sim \lambda$, then the average number of dipoles, and the variance grow according to

$$\langle n(y)\rangle \approx e^{\lambda y}, \tag{20}$$

$$V(y) \equiv \langle n^2\rangle - \langle n\rangle^2 \approx e^{2\lambda y} - e^{\lambda y} = \langle n\rangle^2(1 - e^{-\lambda y}). \tag{21}$$

Thus the distribution satisfies approximate KNO scaling.

For two colliding cascades, evolved to rapidities y_1 and y_2 respectively, we have $s \approx \exp(y_1 + y_2) = \exp(Y)$, with $Y \equiv y_1 + y_2$. Assuming a dipole-dipole interaction probability $2f$, we get for the bare pomeron exchange (neglecting unitarization effects)

$$\sigma_{inel} \propto e^{\lambda y_1}\, 2f\, e^{\lambda y_2} = 2f\, e^{\lambda Y} = 2f\, s^{\lambda}, \tag{22}$$

$$\sigma_{el} \propto f^2 e^{2\lambda Y} = f^2 s^{2\lambda}. \tag{23}$$

This corresponds to a pomeron intercept $\alpha(0) = 1 + \lambda$

In the *triple-regge* formalism, the triple-pomeron diagram in fig. 13 gives the following result for the integrated single diffractive cross section with $M_X^2 < M_{max}^2 \approx \exp(y_1)$:

$$\int_{(M<M_{max})} \frac{d\sigma_{SD}}{d\ln M^2} dy_1 = f^2\, e^{2\lambda Y}(1 - e^{-\lambda y_1}) = f^2\, s^{2\lambda}(1 - 1/(M_{max}^2)^{\lambda}). \tag{24}$$

In the *Good–Walker* formalism this cross section is determined by the fluctuations. For projectile excitation but intact target we obtain

$$\sigma_{\rm SD} = \langle\langle T\rangle_{\rm targ}^2\rangle_{\rm proj} - \langle\langle T\rangle_{\rm targ}\rangle_{\rm proj}^2 = f^2 e^{2\lambda Y}(1 - e^{-\lambda y_1}). \tag{25}$$

We see that we get exactly the same expression in the two approaches. Most essential for this result is the approximate KNO scaling.

We also note that the DIPSY results, calculated with the Good–Walker formalism, have the expected triple-pomeron form. The results for total, elastic, and single-diffractive cross sections, calculated for the *bare* pomeron (meaning the Born amplitude without saturation effects) are shown in fig. 14. We see that the cross sections grow

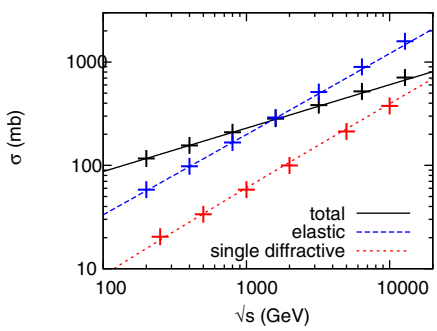

Figure 14. DIPSY result for cross sections before unitarization [17].

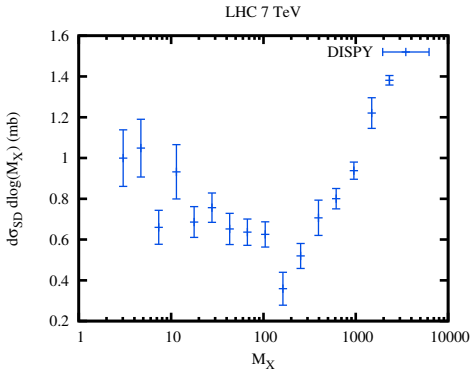

Figure 15. Preliminary results from DIPSY for $d\sigma_{SD}/d\ln M_X$ at 7 TeV.

as powers of s, in accordance with a regge fit with a single pomeron pole with parameters

$$\alpha(0) = 1.21, \quad \alpha' = 0.2\,\mathrm{GeV}^{-2} \tag{26}$$

$$g_{pP}(t) = (5.6\,\mathrm{GeV}^{-1})\, e^{1.9t} \tag{27}$$

$$g_{3P}(t) \approx 1\mathrm{GeV}^{-1} \ \text{(dep. on def.)} \tag{28}$$

We note also that when unitarization is omitted, the elastic cross section is larger than the total for $\sqrt{s} > 2$ TeV.

Fig. 15 shows preliminary results for $d\sigma_{SD}/d\ln M_X$ at 7 TeV, which should be compared with the LHC data in fig. 7. (Note that the diffractive mass grows in opposite directions in the two figures.)

4 Hard diffraction

Factorization and factorization breaking

UA8 at the CERN $S\,p\bar{p}S$ collider (consisting of the UA2 central detector plus roman pots at 630 GeV) observed high $p_\perp$ jets in diffractive events [19]. Jets have also been observed in gap events at HERA and the Tevatron. These events are often analyzed within the Ingelman–Schlein model [20], which assumes that the pomeron has a universal parton substructure $f^P_{q,g}(z, Q^2)$. This implies that the diffractive cross section factorizes (*cf* fig. 16):

$$\sigma^{diff} \sim \sum_i F^p_P(x_P) \otimes f^P_i(z = x_{Bj}/x_P, Q^2) \otimes \hat{\sigma}_{\gamma^* i}. \tag{29}$$

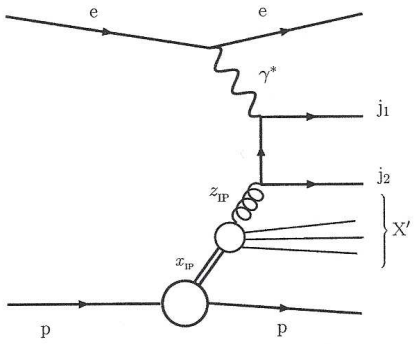

Figure 16. A diagram for hard diffraction in the Ingelman–Schlein model.

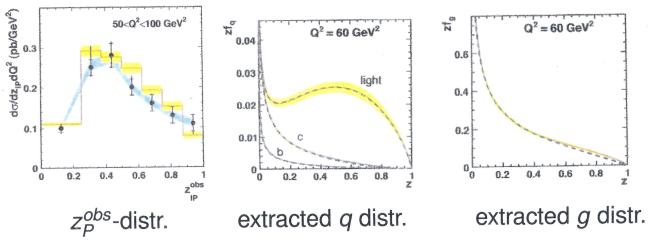

Figure 17. Pomeron pdf:s determined by ZEUS, together with a comparison with data for the distribution in the observed parton fraction of the pomeron momentum, z_P^{obs} [21].

Here x_P is the energy fraction carried by the pomeron, and the sum runs over different parton species i.

A fit with DGLAP evolution to HERA DIS data for hard and soft diffraction by ZEUS [21] is shown in fig. 17, together with a comparison with data for the distribution in the observed parton fraction of the pomeron momentum, z_P^{obs}. We note in particular that the distributions are gluon dominated. The Ingelman–Schlein model is implemented in a number of MC generators, *e.g.* POMPYT, PYTHIA8, and POMWIG.

Factorization was proved by Collins for hard scattering in DIS [22]. Results from the Tevatron showed, however, that factorization is strongly broken when comparing diffractive two-jet events in DIS and pp collisions [23]. In pp scattering the gaps become frequently filled by soft interactions. Figure 18 shows the ratio between single diffractive and non-diffractive events ($R = SD/ND$) from CDF, which are a factor 0.1 – 0.2 below the corresponding DIS data. Similarly fig. 19 shows a fit to data for $dN/d\tilde{\xi} \approx dN/d(M_X^2/s)$, where the pomeron flux is renormalized in the MC with a gap survival probability ≈ 0.2 [24].

Similarities between diffractive and non-diffractive scattering

CDF has noted that there are strong similarities between jet production in single diffractive and non-diffractive events, hinting at a similar dynamical origine. Fig. 20 shows the distribution of two-jet events *vs* mean

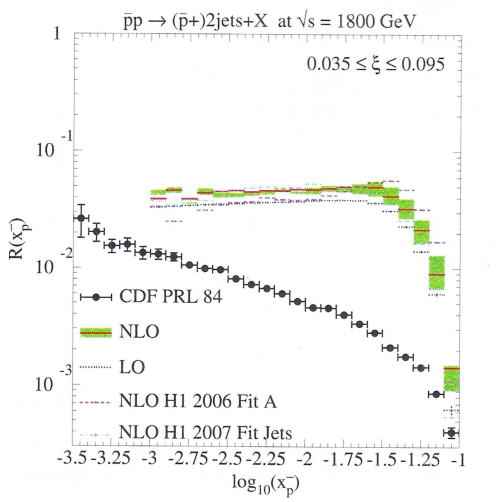

Figure 18. The ratio $R = SD/ND$. Data from CDF compared to expectation from NLO fit to HERA data, assuming factorization [25].

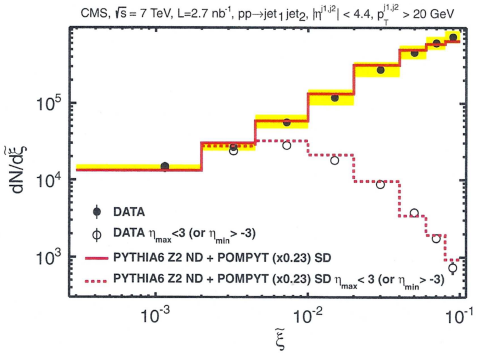

Figure 19. Data on $d\tilde{N}/d\tilde{\xi} \approx dN/d(M_X^2/s)$ measured by CMS, compared with expectations with a pomeron flux rescaled by a factor 0.2 [24].

$E_\perp$, for diffractive and non-diffractive events, which indicates that the same hard subprocess is at work. There is a gap survival probability S^2, but *no extra suppression* $\sim 1/Q^2$ *for diffractive events*. This is consistent with Goulianos' empirical "renormalized pomeron" [26], and also with the assertion that hard diffraction is leading twist by Kopeliovich *et al.* [27].

The gap survival probability for multiple gaps is difficult to calculate. Some processes with multiple gaps are shown in fig. 21. CDF has studied the ratios 2-gap/no-gap (SDD/SD) and one-gap/no-gap (DD/tot). The results, reproduced in fig. 22, show that *multiple gaps are not multiply suppressed*. This feature is also consistent with Goulianos' renormalized pomeron [26].

Central exclusive production

Many schemes are proposed for gap survival in central exclusive production (see *e.g.* refs. [31–34]).

Fig. 23 shows a diagram including eikonal and enhanced survival factors from the Durham group. Gap survival factors have been determined from experimental data for $Q\bar{Q}$ and two-jet production. As a rule of thumb they are approximately 0.2 – 0.3 at the Tevatron, reduced to ~ 0.03 at LHC.

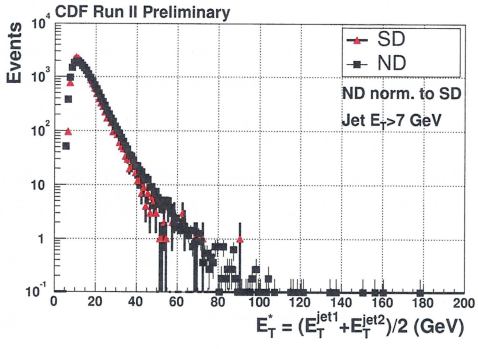

Figure 20. The distribution of diffractive and non-diffractive two-jet events *vs* mean $E_\perp$, measured by CDF (from Goulianos, proc. 13th Blois Workshop, 2009 [28].)

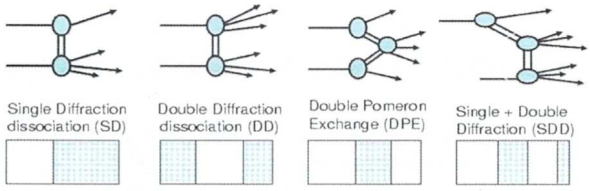

Figure 21. Different processes with multiple gaps. (Figure from Goulianos, proc. 13th Blois Workshop, 2009 [28].)

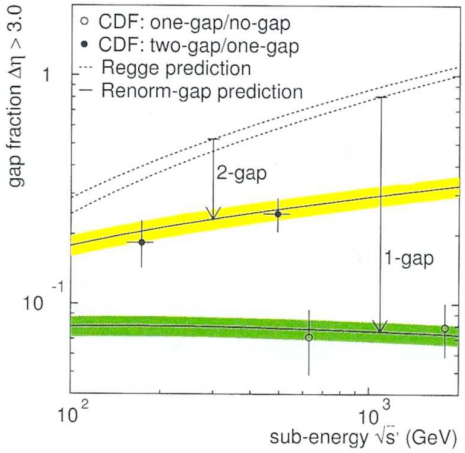

Figure 22. Ratios 2-gap/no-gap and one-gap/no-gap, compared to a regge prediction and the prediction from a renormalized pomeron [29].

Interesting processes for further studies include:

- Comparison between W^+W^- and jet-jet states, which can determine the relation between quarks and gluons in the pomeron.

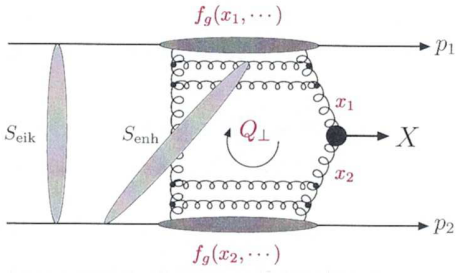

Figure 23. Diagram for hard central production from KMR, with eikonal and enhanced survival factors. (Figure from ref. [30].)

- Jet–gap–jet events in double diffraction, as a means to study BFKL evolution.
- Study $\gamma\gamma \to \gamma\gamma$ or $\gamma\gamma \to W^+W^-$, which can give information about possible anomalous weak couplings.
- Higgs search.

5 Conclusions

Soft diffraction

Several groups have presented analyses of elastic and diffractive cross sections within the Regge formalism. They can contain either one pomeron (GLM), a soft and a hard pomeron (Ostapchenko), or a pomeron interpolating between soft and hard (KMR). Unitarization is taken into account by summation of pomeron loop diagrams, where the results also depend on the assumptions made for multi-pomeron vertices, which vary between the groups. For lower masses, M_X, contributions from low-lying reggeon trajectories are also important, and have to be included with extra parameters. The Regge-based formulations also generally include production of low mass N^* resonances within the Good–Walker formalism, approximating it with two or three diffractive eigenstates.

High mass diffraction has, however, also been described using the Good–Walker formalism. The dynamics of BFKL evolution implies large fluctuations, where the gluon multiplicity satisfies approximate KNO scaling. This implies that Good–Walker reproduces the regge form for diffractive excitation. *Thus the triple-pomeron and Good–Walker formalisms actually describe the same physics.* The Good–Walker formalism can here have the advantage that the results do not depend on new tunable parameters.

(When comparing theory with data, we note that at high energies, low mass diffraction is very difficult to measure experimentally, and its behaviour is therefore less well-known.)

Hard diffraction

Hard diffraction is commonly analyzed by means of the Ingelman–Schlein formalism, assuming a factorized form with a partonic structure for the pomeron. Factorization is, however, strongly broken when comparing data for pp and γp scattering, due to soft exchange in pp reactions. The survival probability in pp collisions is estimated to $\sim 0.1 - 0.2$ at the Tevatron, and ~ 0.03 at LHC.

Data from the Tevatron indicate that the same hard subprocess is at work in diffractive and non-diffractive hard processes, and that multiple gaps are not multiply suppressed. These features are in agreementt with Goulianos' empirical renormalized pomeron.

The LHC detectors have larger acceptance in rapidity than the detectors at HERA or the Tevatron, which implies that we can look forward to many interesting analyses using roman pots at the LHC.

References

[1] E. Luna, V. Khoze, A. Martin, M. Ryskin, Eur.Phys.J. **C59**, 1 (2009), 0807.4115
[2] E. Gotsman, E. Levin, U. Maor (2014), 1403.4531
[3] V. Khoze, A. Martin, M. Ryskin (2014), 1402.2778
[4] S. Ostapchenko, Phys.Rev. **D83**, 014018 (2011), 1010.1869
[5] G. Antchev et al. (TOTEM Collaboration), Europhys.Lett. **101**, 21002 (2013)
[6] N. Cartiglia (2013), 1305.6131
[7] G. Aad et al. (ATLAS Collaboration), Eur.Phys.J. **C72**, 1926 (2012), 1201.2808
[8] A.H. Mueller, Nucl.Phys. **B415**, 373 (1994)
[9] A.H. Mueller, B. Patel, Nucl.Phys. **B425**, 471 (1994), hep-ph/9403256
[10] E. Avsar, G. Gustafson, L. Lonnblad, JHEP **0507**, 062 (2005), hep-ph/0503181
[11] E. Avsar, G. Gustafson, L. Lonnblad, JHEP **0701**, 012 (2007), hep-ph/0610157
[12] C. Flensburg, G. Gustafson, L. Lonnblad, JHEP **1108**, 103 (2011), 1103.4321
[13] C. Flensburg, G. Gustafson, L. Lonnblad, Eur.Phys.J. **C60**, 233 (2009), 0807.0325
[14] H.I. Miettinen, J. Pumplin, Phys.Rev. **D18**, 1696 (1978)
[15] Y. Hatta, E. Iancu, C. Marquet, G. Soyez, D. Triantafyllopoulos, Nucl.Phys. **A773**, 95 (2006), hep-ph/0601150
[16] E. Avsar, G. Gustafson, L. Lonnblad, JHEP **0712**, 012 (2007), 0709.1368
[17] C. Flensburg, G. Gustafson, JHEP **1010**, 014 (2010), 1004.5502
[18] G. Gustafson, Phys.Lett. **B718**, 1054 (2013), 1206.1733
[19] R. Bonino et al. (UA8 Collaboration), Phys.Lett. **B211**, 239 (1988)
[20] G. Ingelman, P. Schlein, Phys.Lett. **B152**, 256 (1985)
[21] S. Chekanov et al. (ZEUS Collaboration), Nucl.Phys. **B831**, 1 (2010), 0911.4119
[22] J.C. Collins, Phys.Rev. **D57**, 3051 (1998), hep-ph/9709499
[23] T. Affolder et al. (CDF Collaboration), Phys.Rev.Lett. **84**, 5043 (2000)
[24] S. Chatrchyan et al. (CMS Collaboration), Phys.Rev. **D87**, 012006 (2013), 1209.1805

[25] M. Klasen, PoS **DIS2010**, 073 (2010), 1005.3948
[26] K.A. Goulianos, Phys.Lett. **B358**, 379 (1995), hep-ph/9502356
[27] B. Kopeliovich, I. Potashnikova, I. Schmidt, A. Tarasov, Phys.Rev. **D76**, 034019 (2007), hep-ph/0702106
[28] M. Deile, D. d'Enterria, A. De Roeck (2010), 1002.3527
[29] D. Acosta et al. (CDF Collaboration), Phys.Rev.Lett. **91**, 011802 (2003), hep-ex/0303011
[30] M. Ryskin, A. Martin, V. Khoze, Eur.Phys.J. **C60**, 265 (2009), 0812.2413
[31] V. Khoze, A. Martin, M. Ryskin, Eur.Phys.J. **C23**, 311 (2002), hep-ph/0111078
[32] J.R. Forshaw (2005), hep-ph/0508274
[33] B. Cox, A. Pilkington, Phys.Rev. **D72**, 094024 (2005), hep-ph/0508249
[34] M. Boonekamp, A. Dechambre, V. Juranek, O. Kepka, M. Rangel et al. (2011), 1102.2531